Modeling Dispersion and Radiation Characteristics of Conductor-Backed CPW With Finite Ground Width

Frank Schnieder, Thorsten Tischler, *Student Member, IEEE*, and Wolfgang Heinrich, *Senior Member, IEEE*

***Abstract*—Dispersion and radiation properties of the conductor-backed coplanar waveguide (CPW) with finite ground planes are analyzed and modeled. A frequency-domain finite-difference method using the perfectly matched layer absorbing boundary condition is used as reference. Based on these results, a closed-form description is derived and implemented into an existing quasi-static CPW model. This leads to a comprehensive and efficient CPW description accounting for all relevant effects from conductor loss to high-frequency dispersion. Additionally, design rules to avoid parasitic radiation effects are given.**

***Index Terms*—Coplanar waveguide (CPW), leaky waves, modeling, radiation effects.**

I. Introduction

LEAKAGE phenomena and higher order modes in coplanar and slot lines have been the subject of investigation for more than ten years (e.g., [1]–[3]). With commercial systems reaching the W-band, dispersion, and radiation properties of coplanar waveguides (CPWs) have become essential topics for practical circuit design. Typical questions, for instance, refer to design rules for the width of CPW ground planes or proper values of substrate thickness, given a certain frequency range of operation.

Most of the publications so far treat coplanar structures on a suspended (or infinite) substrate [2]–[4] and, in many cases, with laterally infinite ground planes [3], [4]. The focus in practical monolithic microwave integrated circuit (MMIC) applications, however, is on the conductor-backed type and, naturally, on ground planes of finite lateral extent. Recently, the authors explained the behavior of this type of CPW in a more qualitative manner [5]. In this paper, modeling equations for the dispersion and radiation effects are supplied, which can be applied for practical circuit design. We expand the quasi-static equivalent-circuit CPW model [6] to include these effects. A radiation resistance $R'_{\rm rad}$ representing the radiation losses of the CPW is added to the original resistance R' representing the conductor losses. The original capacitance C' in the model is modified in order to account for dispersion at higher frequencies.

Fig. 1 shows the CPW cross section that the following considerations are based upon. A conductor-backed (high-resistivity) Si substrate is assumed as an example. Since we are concentrating on dispersion and radiation effects, metal thickness and material losses are neglected in order to separate radiation from other loss phenomena. Regarding the dimensions, values typical for millimeter-wave MMICs are chosen (50-Ω characteristic impedance, 4-μm ground-to-ground spacing). A finite-difference frequency-domain (FDFD) code using the perfectly matched layer (PML) boundary to simulate open space [7] was used as a reference for our simplified model.

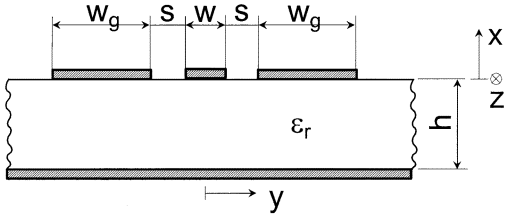

Fig. 1. Cross section of the conductor-backed CPW structure under investigation (the dimensions and material data are, unless otherwise specified, $\varepsilon_r = 11.67$, $w = 16\ \mu$m, $s = 12\ \mu$m, metal thickness $t = 0$, $w_g = 80\ \mu$m, $h = 200\ \mu$m). Further parameters are ground-to-ground-spacing $d = w + 2s$ and total linewidth $w_{\rm tot} = d + 2w_g$. For full-wave EM analysis (FDFD method), the structure is enclosed in a box with lateral and top boundaries realized as the PML.

II. CPW Dispersion

Applying the FDFD method, a systematic study of the CPW dispersion properties as a function of dimensions and material data was performed. CPW effective permittivity $\varepsilon_r = (\beta/\beta_0)^2$ was calculated varying the dimensions w, s, w_g, substrate thickness h, and relative dielectric constant ε_r. The objective was to sort out the important parameters and to describe the dependence of $\varepsilon_{r,\,\rm eff}$ on these quantities by an analytical formula. The investigation reveals that CPW dispersion is almost independent of the substrate thickness h for the parameter range of practical interest. Moreover, $\varepsilon_{r,\,\rm eff}$ depends only on the ratio $d/w_{\rm tot}$ and on frequency f with f being normalized to f_{g1}. The quantity $w_{\rm tot} = w + 2s + 2w_g$ denotes the total width of the CPW and $d = w + 2s$ denotes the ground-to-ground spacing.

The limiting frequency f_{g1} corresponds to the frequency, where the phase constants of the CPW mode and the first lateral higher order mode intersect. A simple approximation is employed, i.e., for the CPW mode, the quasi-static $\varepsilon_{r,\,\rm eff}$ value $\varepsilon_q = (\varepsilon_r + 1)/2$ is used. For the higher order mode, the CPW structure is simplified by covering the slots with metal and introducing a vertical magnetic wall at the outer edge of the ground metallization. This leads to a rectangular waveguide cross section with the vertical boundaries being magnetic walls and a width equivalent to half the total width $w_{\rm tot}$ of the CPW ($w_{\rm tot} = w + 2s + 2w_g$) [5] (see Fig. 2). Calculating

Manuscript received September 15, 2001; revised March 1, 2002. This work was supported by the Deutsche Forschungsgemeinschaft under Contract He 1676/10.

The authors are with the Ferdinand-Braun-Institut für Höchfrequenztechnik, D-12489 Berlin, Germany (e-mail: W.Heinrich@ieee.org).

Digital Object Identifier 10.1109/TMTT.2002.806926

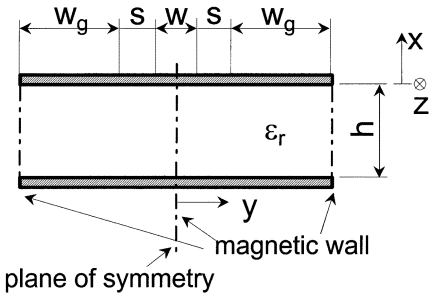

Fig. 2. Simplified CPW structure for the calculation of lateral higher order modes.

the frequency, where $\varepsilon_{r,\,\mathrm{eff}}$ of this waveguide equals ε_q, one obtains f_{g1}

$$f_{g1} = \frac{2}{w_{\mathrm{tot}} \cdot \sqrt{2\mu_0\varepsilon_0(\varepsilon_r - 1)}}. \tag{1}$$

Regarding the dependence on substrate permittivity ε_r, we found, on the basis of FDFD simulations of a large variety of CPW structures, that a normalization of $\varepsilon_{r,\,\mathrm{eff}}$ according to (2) yields good accuracy. Applying

$$\frac{\left(\frac{\varepsilon_{r,\,\mathrm{eff}}}{\varepsilon_q} - 1\right)}{\left(\sqrt{\frac{\varepsilon_r}{\varepsilon_q}} - 1\right)} = p \cdot \left(\frac{f}{f_{g1}}\right)^2. \tag{2}$$

Applying (2), a single fitting parameter p is left, which can be easily determined from a log–log plot and depends only on the ratio d/w_{tot} (with $d = w + 2s$). Using our full-wave simulation data, fitting of p yields

$$p = \frac{2.86465 \cdot \left(\frac{d}{w_{\mathrm{tot}}}\right)^2}{0.15075 + \frac{d}{w_{\mathrm{tot}}}}. \tag{3}$$

Thus, the CPW high-frequency dispersion can be described by the following formula (with $\varepsilon_{r,\,\mathrm{eff}-qs}$ denoting the quasi-static value):

$$\varepsilon_{r,\,\mathrm{eff,\,new}} = \varepsilon_{r,\,\mathrm{eff}-qs} \cdot \left[1 + \left(\sqrt{\frac{\varepsilon_r}{\varepsilon_q}} - 1\right) \cdot p \cdot \left(\frac{f}{f_{g1}}\right)^2\right]. \tag{4}$$

In this way, any quasi-static description can be easily extended to account for dispersion. In our case, we use the quasi-static CPW equivalent-circuit model of [6] and implement (4) by introducing a corresponding modification of line capacitance C'.

III. Radiation for Infinite Substrate Thickness

Studying CPW radiation, one has to distinguish the cases of finite and infinite substrate thickness, which will be treated in Sections III and IV, respectively. First, the structure with the infinite substrate is to be analyzed. In this case, an analytical approximation for radiation loss can be derived. It is based on the approach of Rutledge *et al.* [4], which is adapted here to the CPW with finite-width ground planes.

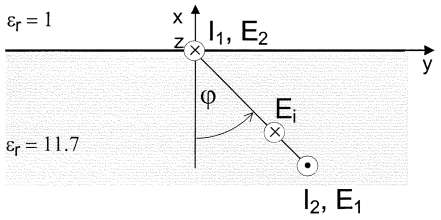

Fig. 3. Reciprocity consideration of an electric line-current source on a dielectric substrate.

Numerical simulations show that, at higher frequencies, α does not vary significantly with substrate thickness h. Therefore, in this range, the expression for infinite h may be used as an approximation for finite h as well, which leads to a simplified formula (see Section IV).

Deriving the analytical model, we follow the common antenna description: first, the field of an infinitesimally small current segment is calculated. Given the current distribution, one then integrates over all segments and, in this way, the total field and, thus, the radiated power is obtained. In our case, the basic current segment is an electric line-current source in the z-direction on the dielectric substrate (see I_1 in Fig. 3).

A. Fields of the Line-Current Source

Due to the layered structure, the fields of the line current in Fig. 3 cannot be derived straightforward. Therefore, we start with the fields of a line current I in a homogeneous medium using cylindrical coordinates (ρ, φ, z). Applying the far-field approximation, the vector potential A_z of a line source, as in Fig. 3, reads (see [8])

$$A_z = \frac{I \cdot e^{-jk_z z}}{\sqrt{8j\pi k\rho}} \cdot e^{jky \cdot \cos(\varphi - (\pi/2))}. \tag{5}$$

$k_z^2 = \omega^2\mu\varepsilon_q$ denotes the propagation constant of the source in the z-direction, which is equal to that of the guided mode (i.e., $\varepsilon_q = \varepsilon_{r,\,\mathrm{eff}}$). The constants k and k_z are related by

$$\omega^2\mu\varepsilon = k^2 + k_z^2 \tag{6}$$

which yields $k^2 = \omega^2\mu\varepsilon_0(\varepsilon_r - \varepsilon_q)$. Consequently, the magnetic and electric fields in the substrate are

$$H_\varphi = j \cdot k \cdot A_z \tag{7}$$

and

$$E_z = -\sqrt{\frac{\mu}{\varepsilon}} \cdot \sin\psi \cdot H_\varphi \tag{8}$$

with

$$\sin\psi = \sqrt{1 - \frac{\varepsilon_q}{\varepsilon_r}}.$$

The next step is to account for the layered medium. This is done following the approach of [4]. Applying the reciprocity theorem to the geometry in Fig. 3, one finds that the field E_1 caused by the current I_1 at the dielectric–air interface at $x = y = 0$ is the same as the field E_2 induced by an artificial current I_2 within the substrate. The latter one is easier to calculate since the incident field E_{zi} at $x = y = 0$ is given by (8). In

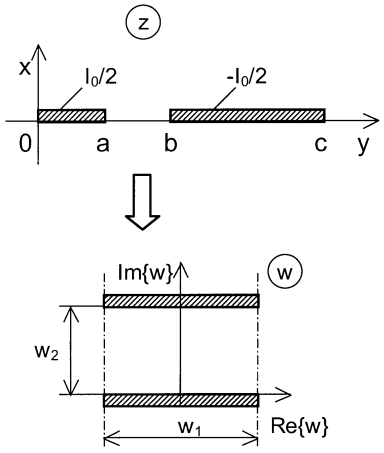

Fig. 4. Conformal mapping for a CPW with finite-extent ground planes.

order to obtain the total field E_{z2}, reflection and transmission at the interface $x = 0$ need to be accounted for. With τ being the transmission coefficient of the z component of E_i at the interface [4], one has for the total electric field E_{z2}

$$E_{z2} = \tau \cdot E_{zi}. \tag{9}$$

According to reciprocity, E_{z2} is equal to the field E_{z1} generated by the current source at $x = y = 0$ that we are looking for with E_{zi} given by (8).

B. CPW Current Distribution

Assuming a CPW with zero-thickness metallizations and quasi-TEM behavior, the current density $J_z(y)$ for $y \geq 0$ can be derived from the conformal mapping of the first quadrant of Fig. 1 into a parallel-plate capacitor, as illustrated by Fig. 4 (see [9])

$$\begin{aligned} J_z(y) &= \frac{dI}{dy} \\ &= \frac{dI}{dw} \cdot \frac{dw}{dy} \\ &= \frac{I}{w_1} \cdot \frac{2j}{\sqrt{(y^2-a^2)\cdot(y^2-b^2)\cdot(y^2-c^2)}} \end{aligned} \tag{10}$$

with I denoting the total current on the right-hand half of the center strip and the right-hand ground metallization ($I = I_0/2$ and $-I_0/2$, respectively)

$$w_1 = \frac{2 \cdot K(r)}{\sqrt{b^2(c^2-a^2)}} \quad r = \frac{a}{b} \cdot \sqrt{\frac{c^2-b^2}{c^2-a^2}}$$

and $K(r)$ denoting the complete elliptic integral of the first kind.

C. Integration

The total field arises from the superposition of all current segments weighted by the actual current distribution. This results in an integration for the electric field according to (11)

$$\begin{aligned} E_z^{(\text{total})} = -\sqrt{\frac{\mu}{\varepsilon}} \cdot \sqrt{1-\frac{\varepsilon_{r,\,\text{eff}}}{\varepsilon_r}} \cdot \frac{j\cdot k \cdot e^{-jk_z z}}{\sqrt{8j\pi k\rho}} \\ \cdot \int_{-\infty}^{+\infty} J_z(y) \cdot e^{jky\cdot\cos(\varphi-(\pi/2))}\, dy \end{aligned} \tag{11}$$

where the current density $J_z(y)$ follows from (10) and is nonzero on the strips only. In order to solve the integral in (11), we split the integration at $y = 0$ and use the symmetry $J_z(y) = J_z(-y)$ (this integral is referred to as Int) as follows:

$$\begin{aligned} \text{Int} &= \int_{-\infty}^{+\infty} J_z(y) \cdot e^{jky\cdot\sin\varphi}\, dy \\ &= \int_0^{\infty} J_z(y) \cdot \left[e^{jky\cdot\sin\varphi} + e^{-jky\cdot\sin\varphi}\right] dy \\ &= 2 \cdot \int_0^{\infty} J_z(y) \cdot \cos(ky\cdot\sin\varphi)\, dy. \end{aligned} \tag{12}$$

For small arguments (as is the case here), the cosine function can be approximated by the first two terms of its series expansion, which yields

$$\text{Int} = 2 \cdot \left\{ \int_0^{\infty} J_z(y)\, dy - \frac{1}{2} \int_0^{\infty} J_z(y) \cdot k^2 \cdot y^2 \cdot \sin^2\varphi\, dy \right\}. \tag{13}$$

Since under quasi-TEM conditions the net current vanishes [see (10)], the first integral in (13) is zero for the CPW and only the second integral with the square term in k needs to be evaluated. This is in contrast to the classical case of infinite ground planes [4], where the first nonvanishing term is the linear one and not the square one.

D. Radiation Loss and Attenuation

From the total fields, the power loss due to radiation into the substrate can be calculated as follows:

$$P_{\text{loss}} = -\frac{1}{2} \int_{-\pi/2}^{\pi/2} |\tau|^2 \cdot E_z \cdot H_{\varphi}^{*} \cdot \rho \cdot d\varphi. \tag{14}$$

This power loss is introduced into the equivalent-circuit model of the CPW [6] by an additional radiation resistance R'_{rad} in the series branch ($P_{\text{loss}} = R'_{\text{rad}} \cdot I_0^2/2$). Using the approximation for $|\tau|^2$ for $\varepsilon_r \geq 4$ in [4]

$$|\tau|^2 = \frac{4\cos^2\varphi}{1+\sin^2\varphi} \tag{15}$$

we obtain the expression

$$\begin{aligned} R'_{\text{rad}} = \frac{\mu_0^3 \cdot \varepsilon_0^2 \cdot \omega^5}{16 \cdot \varepsilon_r} \cdot (\varepsilon_r - \varepsilon_q)^3 \cdot \left(\sqrt{8} - 2.75\right) \\ \cdot \left\{ \left(b^2 - a^2\right) \cdot \left[\frac{K(r) - \Pi(r_1,\, r) - \Pi(r_2,\, r)}{K(r)} \right] \right\}^2 \end{aligned} \tag{16}$$

with $a = w/2$, $b = w/2 + s$, $c = w/2 + s + w_g$, $r_1 = a/b$

$$r_2 = \sqrt{\frac{c^2-b^2}{c^2-a^2}}$$

$r = r_1 \cdot r_2$, the complete elliptical integral of the first kind $K(r)$, and the complete elliptical integral of the third kind $\Pi(n,\, m)$.

If direct results on attenuation α and not on the radiation resistance are required, attenuation can be calculated from the ratio of radiated power P_{loss} to the power transmitted on the line. Note that attenuation of a CPW with finite ground width shows a f^5 dependence in contrast to the attenuation of a CPW with infinite ground width, which follows a f^3 rule.

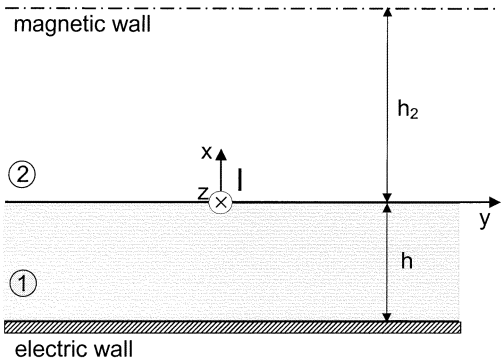

Fig. 5. Model used to calculate radiation of a conductor-backed CPW analytically. Medium 1 refers to the substrate with relative dielectric constant ε_r, for medium 2 it holds $\varepsilon_r = 1$; thickness h_2 is chosen large compared to substrate thickness h such that the influence of the top boundary can be neglected.

IV. Radiation for Finite Substrate Thickness

In the case of the coplanar structure according to Fig. 1, leakage occurs due to surface waves on a conductor-backed dielectric slab of thickness h. The leakage starts at a frequency $f_{g2} > 0$, where the phase constant of the CPW mode becomes smaller than that of the first surface wave [1], [9] (note that this differs from the classical case of a CPW with infinitely thick substrate, where radiation starts at $f = 0$). Below f_{g2}, radiation is zero because the phase constant of the CPW mode is larger than those of the surface waves and, hence, no coupling occurs:

$$f_{g2} = \frac{\arctan(\varepsilon_r)}{\pi \cdot h \cdot \sqrt{2 \cdot \mu_0 \cdot \varepsilon_0 \cdot (\varepsilon_r - 1)}}. \tag{17}$$

In a first approximation, radiation loss of a conductor-backed CPW can be described by a two-region approach with R'_{rad} being zero below f_{g2} and assuming the value of the case for infinitely thick substrate above [see (16)]. This is confirmed by FDFD simulations, but, as can be expected, accuracy of this simple approach is crude around f_{g2}. A more accurate description, which is nevertheless efficient enough to be suitable for circuit design software, is presented below.

The assumptions are similar to those of the model in Section III. Fig. 5 illustrates the geometry. An upper magnetic wall is introduced, far enough away to prevent a parasitic influence. However, due to the upper boundary, one has a discrete eigenmode spectrum, which facilitates analysis. The electric and magnetic fields are expanded into longitudinal-section electric (LSE) and longitudinal-section magnetic (LSH) modes [11]. These LSE and LSH modes propagate in the $\pm y$-direction. The eigenvalue equation of the LSE_x modes reads (the superscripts denote the medium according to Fig. 5)

$$\frac{k_x^{E(1)}}{\varepsilon_r} \cdot \tan\left(k_x^{E(1)} \cdot h\right) = k_x^{E(2)} \cdot \cot\left(k_x^{E(2)} \cdot h_2\right) \tag{18}$$

with

$$k_x^{E(2)} = \sqrt{\left(k_x^{E(1)}\right)^2 - \omega^2 \mu_0 \varepsilon_0 (\varepsilon_r - 1)} \tag{19}$$

because, as a consequence of continuity, the propagation constant k_y is identical in substrate and in air (mediums 1 and 2). Similarly, the eigenvalue equation of the LSH_x modes is

$$k_x^{H(1)} \cdot \cot\left(k_x^{H(1)} \cdot h\right) = k_x^{H(2)} \cdot \tan\left(k_x^{H(2)} \cdot h_2\right) \tag{20}$$

with $k_x^{H(2)}$ according to (19) with the superscript E being replaced by H.

The eigenvalue equations (18)–(20) cannot be solved analytically. Thus, an iterative root search procedure needs to be applied. The problem is that one has to guarantee completeness, i.e., to make sure that all eigenvalues in a given interval are found. This can be accomplished by applying appropriate starting values for the root search. Brandis *et al.* [12] published a method to generate intervals for such a layered structure, which contain exactly one eigenvalue. This is applied here to obtain a reliable and automatized algorithm determining the LSE_x and LSH_x eigenvalues. For details, see Appendix A. Using these intervals as starting values, the root search is performed by successive division of intervals, accounting for possible resonance points and treating the two possible cases of real and imaginary $k_x^{E,H(2)}$ separately.

After the eigenvalues k_{xm} have been determined, the propagation constants of the LSE and LSH modes in the $+y$- and $-y$-direction are calculated according to (21)

$$k_{ym}^{E,H} = \sqrt{\omega^2 \mu_0 \varepsilon_0 \varepsilon_r - \left(k_{xm}^{E,H(1)}\right)^2 - k_z^2} \tag{21}$$

with k_z as introduced in (5). Only modes with a real $k_{ym}^{E,H}$ propagate and, thus, contribute to radiation. This corresponds to $k_x^{E,H(1)}$ being in the range

$$0 < k_{xm}^{E,H(1)} \leq \sqrt{\omega^2 \mu_0 \varepsilon_0 \varepsilon_r - k_z^2}. \tag{22}$$

Thus far, we know only the properties of the LS modes, but not their amplitudes, i.e., how strong each of them is excited in the given structure. This is determined by the z-directed current line source at the dielectric interface at $y = 0$ (see Fig. 5). Since the eigenfunctions of the LSE and LSH modes are orthogonal, the well-known mode-matching procedure can be applied in order to determine the amplitudes of the LS modes A_m^E and A_m^H, respectively (see Appendix B).

In the last step, power loss of the entire CPW structure due to radiation in the $+y$- and $-y$-direction is calculated by integrating over the current density $J_z(y)$ and adding the contributions of all propagating LSE and LSH modes [see (22)], similar to the procedure in Section III as follows:

$$\begin{aligned} P_{\mathrm{loss}} = \frac{1}{\omega\mu_0} \cdot \sum_{m=1}^{N_H} & k_{ym}^H \cdot \left[\left(k_{ym}^H\right)^2 + k_z^2\right] \cdot \left|A_m^{H(1)}\right|^2 \\ & \cdot YHYH_m \cdot \left[2 \cdot \int_0^\infty \frac{J_z(y')}{I_0} \cdot \cos\left(k_{ym}^H \cdot y'\right) dy'\right]^2 \\ & + \frac{1}{\omega} \cdot \sum_{m=1}^{N_E} k_{ym}^E \cdot \left[\left(k_{ym}^E\right)^2 + k_z^2\right] \cdot \left|A_m^{E(1)}\right|^2 \\ & \cdot YEYE_m \cdot \left[2 \cdot \int_0^\infty \frac{J_z(y')}{I_0} \cdot \cos\left(k_{ym}^E \cdot y'\right) dy'\right]^2. \end{aligned} \tag{23}$$

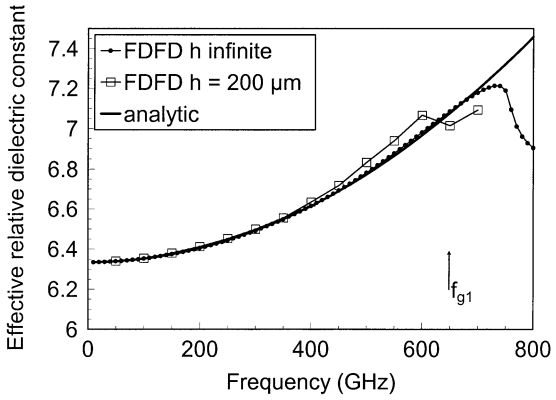

Fig. 6. Effective relative permittivity of the CPW in Fig. 1. Comparison of the analytical model with full-wave FDFD results for finite and infinite substrate thickness. The frequency limit f_{g1} of the analytical model [see (1)] is marked.

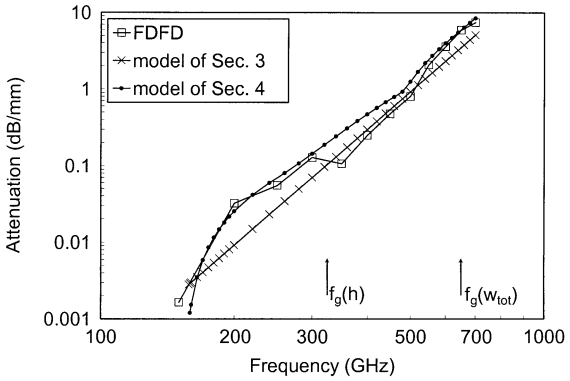

Fig. 7. Attenuation of the CPW in Fig. 1 in double-logarithmic scale (substrate thickness $h = 200\ \mu$m). Comparison of FDFD results with those of the model of Section IV (23) and the description according to (16) in Section III. The frequency limits [(1) and (24)] of the analytical model are included [$f_g(w_{\rm tot})$ is equivalent to f_{g1} in (1)].

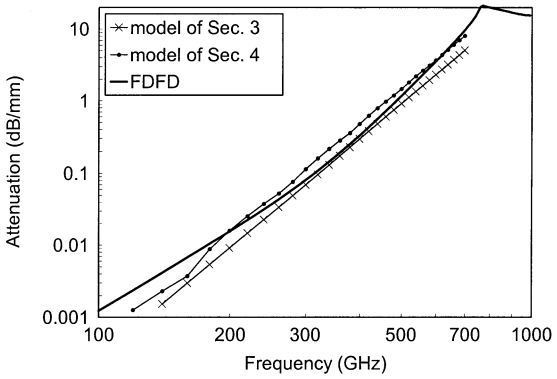

Fig. 8. Attenuation of the CPW in Fig. 1 in double-logarithmic scale (infinite substrate thickness). Comparison of FDFD results with those of the model in Section III and the version for finite thickness in Section IV ($h = 600\ \mu$m is used).

N_H and N_E denote the highest indexes of the respective modes satisfying (22). $J_z(y)$ is defined in (10), the solution of the corresponding integral is closely related to that in (13). As described in Section III, the power loss $P_{\rm loss}$ can be represented by a radiation resistance in the equivalent-circuit model.

V. Accuracy and Limitations of the Extended CPW Model

In this section, results are to be presented for the new CPW model, based on the quasi-static formulation of [6], including high-frequency dispersion and radiation by using (4) and (16) or (23) for infinite or finite substrate thickness, respectively.

Regarding the limitations, one has to note first that the practical range of application of the CPW is restricted to frequencies, where interaction with higher order CPW modes can be neglected. These higher order modes are associated with both lateral line dimensions and substrate thickness [5]. They lead to upper frequency limits $f_g(w_{\rm tot})$ and $f_g(h)$, respectively, with $f_g(w_{\rm tot})$ given in (1) and $f_g(h)$ according to (24) as follows:

$$f_g(h) = \frac{1}{h \cdot \sqrt{2\mu_0\varepsilon_0(\varepsilon_r - 1)}}. \tag{24}$$

This means that both substrate thickness h and total linewidth $w_{\rm tot}$ have to be kept small enough to maintain the desired single-mode CPW behavior. The analytical dispersion and radiation descriptions presented in the previous sections are intended for design purposes and, therefore, focus on this parameter range as well. With growing frequency, their principal validity is limited by f_{g1} in (1).

Fig. 6 presents data on effective permittivity for the CPW structure of Fig. 1. The analytical description of $\varepsilon_{r,\,\rm eff}$ agrees very well with the full-wave FDFD simulations for both finite and infinite substrate thickness. A more systematic investigation yields a maximum deviation of less than 1.5% in $\varepsilon_{r,\,\rm eff}$ (which means 0.75% in phase constant), determined from a variety of CPW geometries. This fully satisfies practical design requirements.

The corresponding attenuation results are plotted in Fig. 7 in a double-logarithmic scale. The approach based on the LS-mode description (23) yields good agreement with FDFD simulations up to the frequency $f_g(h)$, where coupling with the first higher order mode starts and the useful frequency range ends. This validates the new model. As stated in [5] already, a f^5 rule for the frequency is found [see, e.g., (16)]. At frequencies beyond $f_g(h)$, accuracy deteriorates, but the principal characteristics are described further on, though this range should be avoided in practical circuit design [(24) is violated].

Fig. 7 also provides the results of the model for infinite substrate thickness according to (16). This formula gives a rough estimation for attenuation in the case of finite substrate thickness as well. However, as can be expected, it leads to considerable deviations for frequencies in the vicinity of radiation cutoff f_{g2}.

In order to explore this in more detail, Fig. 8 presents the full-wave data for infinite substrate thickness together with the corresponding model (16) and the finite-substrate description of (23) assuming a large thickness $h = 600\ \mu$m. One observes—in the log–log scale—an almost constant difference between both models, i.e., both descriptions do not converge for large substrate thicknesses h. This discrepancy is found for other geometries with strips of finite width as well, e.g., for the coupled-strip line. A physical explanation, however, is yet missing. Additional investigations reveal that the deviations do not occur in the case of infinite metallization width. From this, one may suppose that the approach for the transmission coefficient in (15), which is

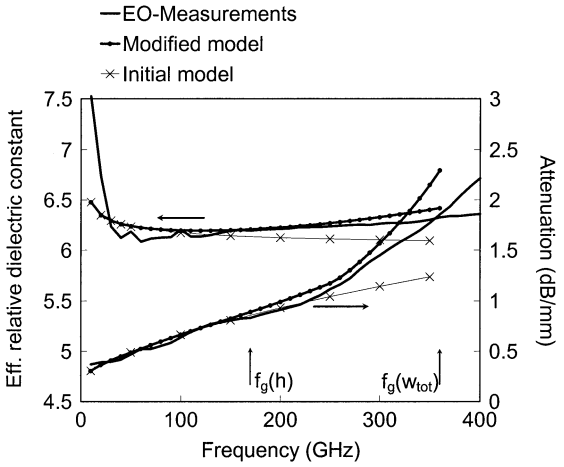

Fig. 9. Effective relative permittivity and attenuation of a CPW according to Fig. 1, but with $w_g = 160\ \mu$m, $h = 380\ \mu$m, gold conductors with thickness $t = 0.8\ \mu$m, and a conductivity of $3.5\ 10^7$ S/m. Comparison of the results of the new model with those of the previous one and with electrooptic measurements.

taken from [4], is responsible for the inaccuracies. Quantitatively speaking, the accuracy of (16) can be significantly improved if we multiply the formula by a correction factor of 1.75.

To check the validity of the new model, we compared the results to electrooptic measurements performed at the RWTH Aachen, Aachen, Germany (see [13]). Fig. 9 presents the results together with those of the initial model [6]. We find that our improved model describes high-frequency dispersion and loss owing to radiation with good accuracy. The deviations in the low-frequency range are due to uncertainties in the electrooptic measurement procedure (transformation from time to frequency domain).

VI. Conclusions

Using the CPW at W-band frequencies and beyond requires careful design of ground width and substrate thickness in order to maintain the desired single-mode behavior with small dispersion and low radiation loss. In this paper, closed-form expressions for CPW high-frequency dispersion and an analytical description for radiation loss have been presented. Using these formulas, the available quasi-TEM equivalent-circuit models of the CPW can be easily extended to cover non-TEM and radiation effects. The results agree well with full-wave data calculated by means of a finite-difference method with absorbing boundaries. The expanded CPW model is numerically very efficient and can be implemented easily as a user-defined model in conventional circuit-design software.

Appendix A
Starting Intervals for the LSE and LSH Root Search

Applying the approach of [12] to the structure of Fig. 5, one obtains a series of intervals for k_x, with each of them containing a single eigenvalue. First, we assume a magnetic wall at the dielectric–air interface separating the structure into two independent subdomains. The conclusion of [12] is that every two neighboring eigenvalues of both subdomains include exactly one eigenvalue of the entire structure.

Thus, the interval boundaries for the eigenvalues of the LSE_x modes consist of $k_x^{E(2)} = n \cdot (\pi/h_2)$ with $n = 1, 2, \ldots,$ and $k_x^{E(1)} = (m + (1/2)) \cdot (\pi/h)$ with $m = 0, 1, 2, \ldots,$ and $k_x^{E(1)} = 0$. The $k_x^{E(2)}$ values can be transformed into the corresponding $k_x^{E(1)}$ values using (19). The resulting $k_x^{E(1)}$ for $n = 1, 2, \ldots,$ and $m = 0, 1, \ldots,$ are written into one sequence ordered by magnitude. Each neighboring $k_x^{E(1)}$ values of this sequence then form the interval containing exactly one eigenvalue.

For the LSH_x modes, the intervals are formed by $k_x^{H(2)} = n \cdot (\pi/h_2)$ with $n = 0, 1, 2, \ldots,$ and $k_x^{H(1)} = (m + (1/2)) \cdot (\pi/h)$ with $m = 0, 1, 2, \ldots$. The remaining part of calculation corresponds to the LSE_x case.

Appendix B
Amplitudes of the LSE and LSH Modes

After some mathematical manipulations, one obtains the following expressions for the amplitudes of the mth LSE_x and LSH_x mode, A_m^E and A_m^H, respectively, in medium 1 (note that orthogonality holds only within the LSE and the LSH system, but not for cross terms):

$$A_m^{H(1)} = +\frac{I_0}{2} \cdot j\omega\mu_0 \cdot \frac{Y_m^{H(1)}(x=0)}{YHYH_m} \cdot \frac{1}{\left(k_{ym}^H\right)^2 + k_z^2} \tag{25}$$

and

$$A_m^{E(1)} = -\frac{I_0}{2} \cdot \frac{k_z}{k_{ym}^E \cdot YEYE_m} \cdot \left(\sum_{n=1}^{\infty} \frac{Y_n^{H(1)}(x=0)}{\left(k_{yn}^H\right)^2 + k_z^2} \cdot \frac{ZHYE_{nm}}{YHYH_n} \right) \tag{26}$$

with

$$YHYH_m = \int_{-h}^{0} \left(Y_m^{H(1)}(x)\right)^2 dx + \left(\frac{Y_m^{H(1)}(x=0)}{Y_m^{H(2)}(x=0)}\right)^2 \cdot \int_0^{h_2} \left(Y_m^{H(2)}(x)\right)^2 dx \tag{27}$$

$$YEYE_m = \frac{1}{\varepsilon_0\varepsilon_r} \cdot \int_{-h}^{0} \left(Y_m^{E(1)}(x)\right)^2 dx + \left(\frac{Y_m^{E(1)}(x=0)}{Y_m^{E(2)}(x=0)}\right)^2 \cdot \frac{1}{\varepsilon_0} \cdot \int_0^{h_2} \left(Y_m^{E(2)}(x)\right)^2 dx \tag{28}$$

$$ZHYE_{nm} = \frac{1}{\varepsilon_0 \cdot \varepsilon_r} \cdot \int_{-h}^{0} Z_n^{H(1)}(x) \cdot Y_m^{E(1)}(x)\, dx + \frac{Y_n^{H(1)}(0) \cdot Y_m^{E(1)}(0)}{Y_n^{H(2)}(0) \cdot Y_m^{E(2)}(0)} \cdot \frac{1}{\varepsilon_0} \cdot \int_0^{h_2} Z_n^{H(2)}(x) \cdot Y_m^{E(2)}(x)\, dx \tag{29}$$

and

$$Y_m^{H(1)}(x) = \sin\left[k_{xm}^{H(1)} \cdot (x+h)\right] \tag{30}$$

$$Y_m^{H(2)}(x) = \cos\left[k_{xm}^{H(2)} \cdot (x-h_2)\right] \tag{31}$$

$$Z_m^{H(1)}(x) = k_{xm}^{H(1)} \cdot \cos\left[k_{xm}^{H(1)} \cdot (x+h)\right] \tag{32}$$

$$Z_m^{H(2)}(x) = -k_{xm}^{H(2)} \cdot \sin\left[k_{xm}^{H(2)} \cdot (x - h_2)\right] \tag{33}$$

$$Y_m^{E(1)}(x) = \cos\left[k_{xm}^{E(1)} \cdot (x + h)\right] \tag{34}$$

$$Y_m^{E(2)}(x) = \sin\left[k_{xm}^{E(2)} \cdot (x - h_2)\right]. \tag{35}$$

The thickness h_2 of the air layer should be large enough so that it does not affect the solution ($h_2 \geq 10 \cdot h$). The same consideration holds for the choice of the number of LSH_x modes used for the calculation of $A_m^{E(1)}$ in (26), which, of course, cannot be infinity in the numerical calculation. This number $N_{\max}^H$ determines how accurate the solution approximates the line current source. Roughly speaking, the spatial resolution is equal to the ratio $(h + h_2)/N_{\max}^H$. In our case, a value $N_{\max}^H = (h + h_2)/4$ μm yielded good accuracy while still maintaining reasonable numerical efforts.

REFERENCES

[1] H. Shigesawa, M. Tsuji, and A. A. Oliner, "Conductor-backed slot line and coplanar waveguide: Dangers and full-wave analyses," in *IEEE MTT-S Int. Microwave Symp. Dig.*, vol. 1, 1988, pp. 199–202.

[2] H. H. Shigesawa, M. Tsuji, and A. A. Oliner, "A new mode-coupling effect on coplanar waveguides of finite width," in *IEEE MTT-S Int. Microwave Symp. Dig.*, vol. 3, 1990, pp. 1063–1066.

[3] M. Y. Frankel, S. Gupta, J. A. Valdmanis, and G. A. Mourou, "Terahertz attenuation and dispersion characteristics of coplanar transmission lines," *IEEE Trans. Microwave Theory Tech*, vol. 39, pp. 910–915, June 1991.

[4] D. B. Rutledge, D. P. Neikirk, and D. P. Kasilingam, "Millimeter components and techniques: Integrated-circuit antennas," in *Infrared and Millimeter Waves*, K. J. Button, Ed. New York: Academic, 1983, vol. 10, ch. 1.

[5] W. Heinrich, F. Schnieder, and T. Tischler, "Dispersion and radiation characteristics of conductor-backed CPW with finite ground width," in *IEEE MTT-S Int. Microwave Symp. Digest*, vol. 3, 2000, pp. 1663–1666.

[6] W. Heinrich, "Quasi-TEM description of MMIC coplanar lines including conductor-loss effects," *IEEE Trans. Microwave Theory Tech*, vol. 41, pp. 45–52, Jan. 1993.

[7] T. Tischler and W. Heinrich, "The perfectly matched layer as lateral boundary in finite-difference transmission-line analysis," *IEEE Trans. Microwave Theory Tech*, vol. 48, pp. 2249–2253, Dec. 2000.

[8] R. F. Harrington, *Time Harmonic Electromagnetic Fields*. New York: McGraw-Hill, 1961, p. 229.

[9] G. Ghione and C. U. Naldi, "Coplanar waveguides for MMIC applications: Effect of upper shielding, conductor backing, finite-extent ground planes, and line-to-line coupling," *IEEE Trans. Microwave Theory Tech*, vol. MTT-35, pp. 260–267, Mar. 1987.

[10] R. K. Hoffmann, *Integrierte Mikrowellenschaltungen*. Berlin, Germany: Springer-Verlag, 1983, pp. 386–389.

[11] R. E. Collin, *Field Theory of Guided Waves*, 2nd ed. New York: IEEE Press, 1991, p. 412.

[12] H. Brandis, U. Crombach, and R. Gesche, "Bounds for the eigenvalues of a multilayered parallel plate line," *Arc. Elektr. Ubertragung.*, vol. 37, no. 3/4, pp. 113–116, 1983.

[13] H.-M. Heiliger, M. Nagel, H. G. Roskos, H. Kurz, F. Schnieder, and W. Heinrich, "Thin-film microstrip lines for mm and sub-mm-wave on-chip interconnects," in *IEEE MTT-S Int. Microwave Symp. Dig.*, vol. 2, 1997, pp. 421–424.

Frank Schnieder was born in Ludwigsfelde, Germany, in 1960. He received the Dipl.-Ing. and Dr.-Ing. degrees in electrical engineering from the Technical University of Dresden, Dresden, Germany, in 1986 and 1990, respectively.

Since 1989, he has been involved with GaAs MMICs. In 1992, he joined the Ferdinand-Braun-Institut für Höchfrequenztechnik (FBH), Berlin, Germany. His current research is focused on MMIC design and transmission-line modeling.

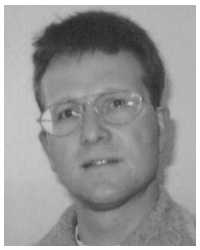

Thorsten Tischler (S'00) was born in Siegen, Germany, in 1968. He received the Diploma degree in electrical engineering from the University of Siegen, Siegen, Germany, in 1997, and is currently working toward the Ph.D. degree at the Ferdinand-Braun-Institut für Höchfrequenztechnik (FBH), Berlin, Germany.

He is currently involved in electromagnetic simulation with a focus on the development of absorbing boundary conditions for the FDFD method.

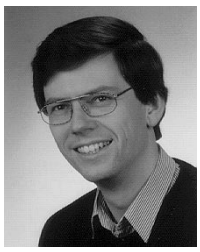

Wolfgang Heinrich (M'84–SM'95) was born in Frankfurt/Main, Germany, in 1958. He received the Dipl.-Ing., Dr.-Ing., and Habilitation degrees from the Technical University of Darmstadt, Darmstadt, Germany, in 1982, 1987, and 1992, respectively.

In 1983, he joined the staff of the Institut für Höchfrequenztechnik, University of Darmstadt, where he was involved with field-theoretical analysis and simulation of planar transmission lines. Since April 1993, he has been with the Ferdinand-Braun-Institut für Höchfrequenztechnik (FBH), Berlin, Germany, where he is currently Head of the Microwave Department. His current research activities focus on electromagnetic simulation, MMIC design for both GaAs and SiGe with emphasis on the coplanar concept, and flip-chip packaging.